Cell Reports, Volume *36*

Supplemental information

Molecular mechanism of cargo recognition and handover by the mammalian signal recognition particle

Ahmad Jomaa, Simon Eitzinger, Zikun Zhu, Sowmya Chandrasekar, Kan Kobayashi, Shu-ou Shan, and Nenad Ban

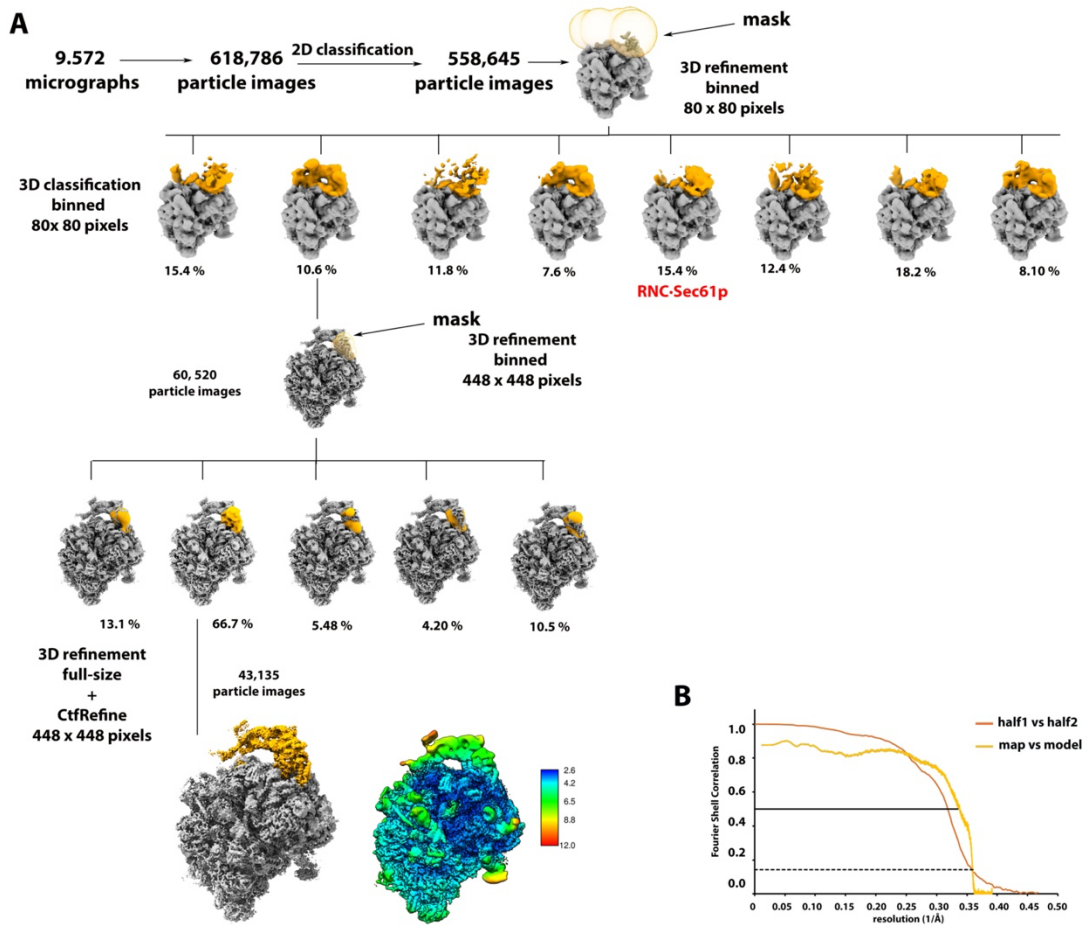

Figure S1. Image classification and refinement of the structure of the early RNC·SRP targeting complex, Related to Figure 1.

(A) An initial 2D classification was performed on binned particles (box size 80 x 80 pixels) to remove bad particles. The selected particle images were then subjected to 3D refinement in RELION3 to obtain an initial map. Using binary mask applied at the ribosome tunnel region, a 3D focused classification without alignment was performed. This approach yielded a 3D class with a density corresponding to the RNC·SRP targeting complex. A second round of focused 3D classification focusing on the SRP proximal site was performed and yielded a 3D class with an improved EM density for SRP. The particles images in the selected class were subjected to a 3D refinement using full size images without binning (448 x 448 pixels) in RELION3, which yielded

a map with an overall resolution of 2.8 Å. Local resolution of RNC·SRP complex (right) was calculated in Relion. **(B)** Fourier Shell Correlation (FSC) plots for the cryo-EM maps shown in panel A and the model versus map plot of the RNC·SRP complex, calculated using the gold standard FSC criteria cutoff (FSC=0.143) using independent two half maps as implemented in RELION3, and the cutoff for the resolution of the model is determined based on the FSC cutoff (FSC=0.5).

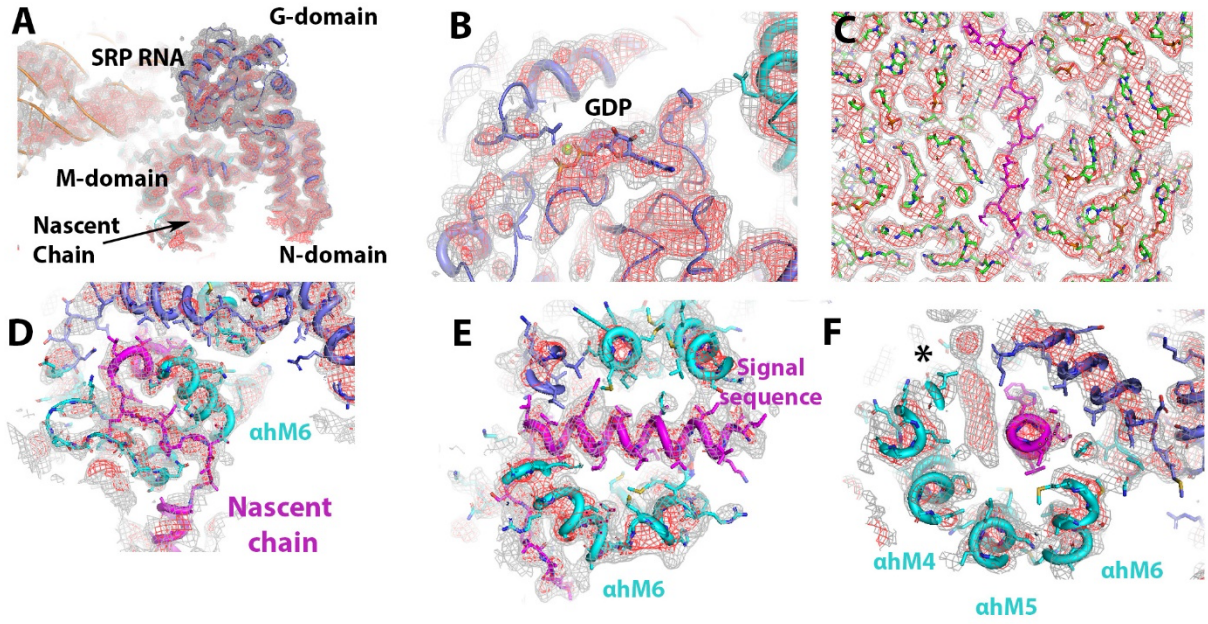

Figure S2. Representative cryo-EM densities of the mammalian SRP targeting complex, Related to Figure 2.

(A) Overview of the EM density of SRP54 NG- and M-domain, signal sequence and SRP RNA. **(B)** Close-up view of the SRP54 G-domain with the bound GDP molecule. **(C)** Cut-through view of the ribosome tunnel with the nascent polypeptide chain. Ribosome is shown as sticks and colored green. Nascent chain is colored magenta. **(D-E)** Representative view of the EM-densities corresponding to the SRP54 M-domain bound (cyan) to the signal sequence (magenta) and the nascent chain as it emerges from the ribosome tunnel. **(F)** Close-up of the M-domain groove including the density of the bound signal sequence and unidentified EM density of a bound molecule inserted into the hydrophobic groove and indicated with an asterisk.

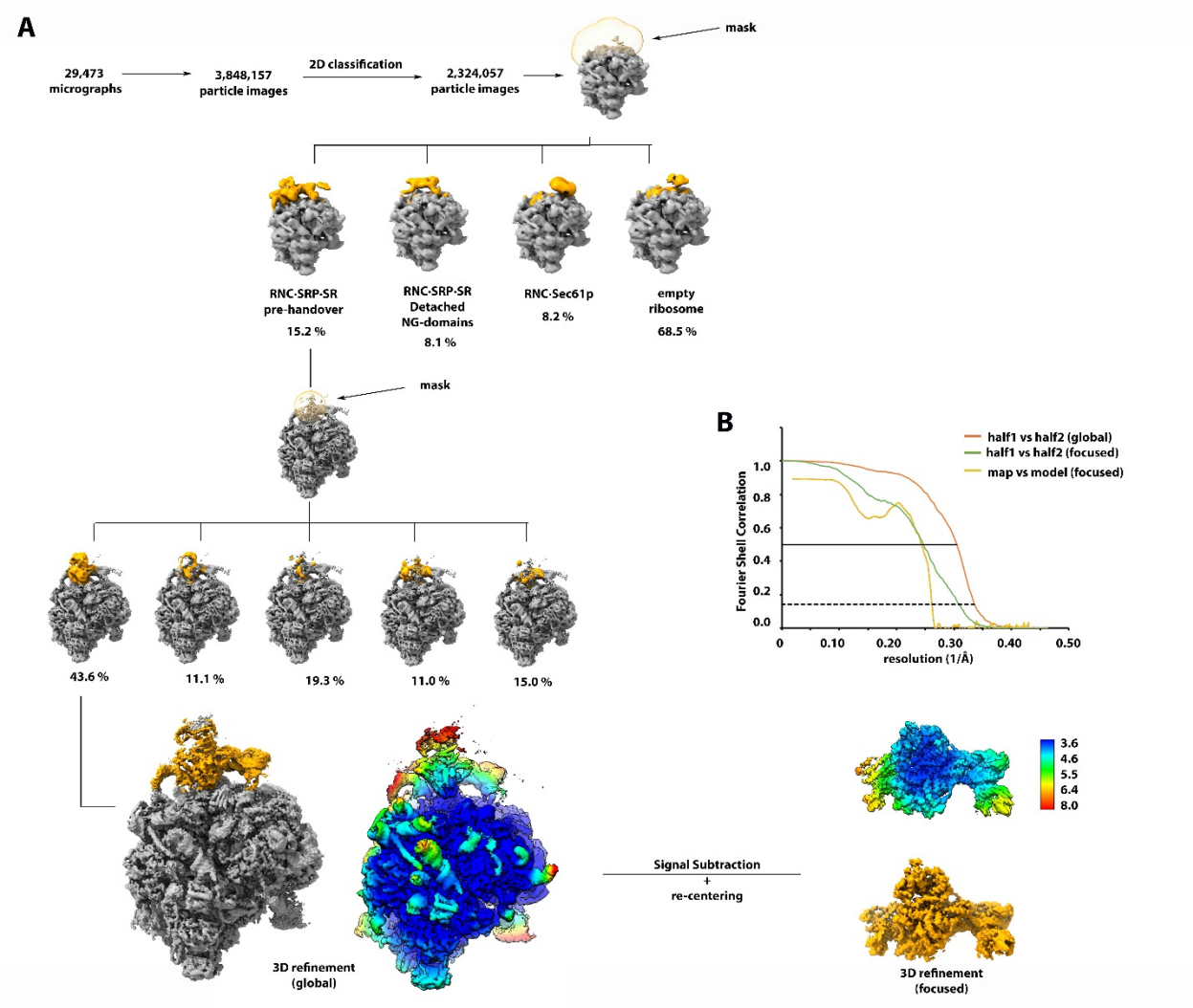

Figure S3. Image classification and refinement of the structure of the late RNC·SRP·SR targeting complex, Related to Figure 1.

(A) An initial 2D classification was performed on binned particles (box size 80 x 80 pixels) to remove bad particles. The selected particle images were then subjected to 3D refinement in RELION3 to obtain an initial map. Using binary mask applied at the ribosome tunnel region, a 3D focused classification without alignment was performed. This approach yielded a 3D class with a density corresponding to the RNC·SRP·SR targeting complex. A second round of focused 3D classification focusing on the SRP distal site was performed and yielded a 3D class with an improved EM density for the SRP·SR complex. The particles images in the selected class were

subjected to a 3D refinement using full size images without binning (448 x 448 pixels) in RELION3, which yielded a map with an overall resolution of 3.0 Å. A final round of 3D refinement was performed after signal subtraction and re-cantering on the density of SRP and SR improved the local resolution to 3.6 - 4.0 Å. Local resolution of SRP·SR complex, based on the global and focused 3D refinements, was calculated in Relion. Local resolution of the focused and global refinements is calculated in Relion. **(B)** Fourier Shell Correlation (FSC) plots for the cryo-EM maps shown in panel a, calculated using the gold standard FSC criteria cutoff (FSC=0.143) using independent two half maps as implemented in RELION3, and for the model versus map plot. The resolution of the model is determined based on the FSC cutoff (FSC=0.5).

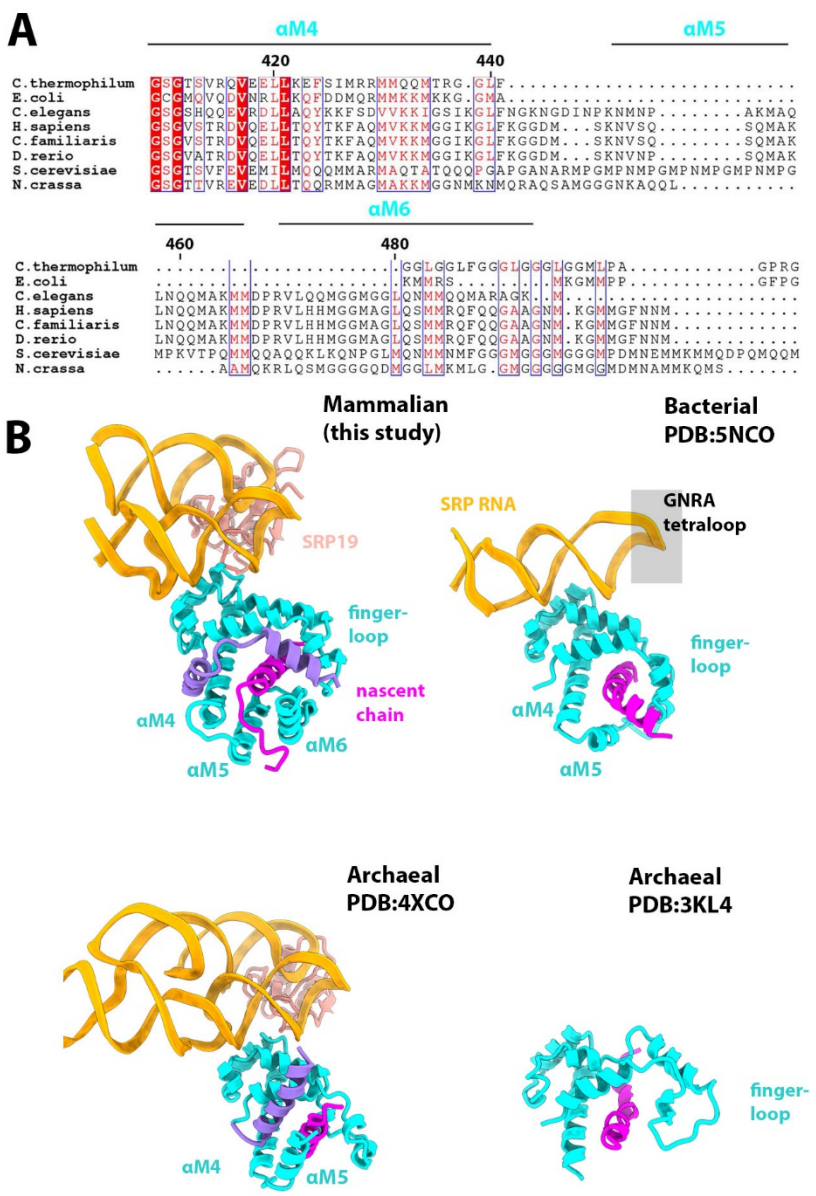

Figure S4. Sequence and structural comparison of the SRP54 M-domain and the signal sequence in bacteria, archaea and eukaryotes, Related to Figure 2.

(A) Sequence alignment of the SRP54 M-domain which is conserved in eukaryotes but is highly variable compared to the bacteria. Sequence alignments were done with the Clustal Omega https://www.ebi.ac.uk/Tools/msa/clustalo/ and displayed with ESPript 3.0

http://espript.ibcp.fr/ESPript/ESPript/. Secondary structural elements of the M-domain indicated are directly visualized in the cryo-EM map of the M-domain determined in this study. **(B)** Overview of the M-domain and the bound signal sequence as visualized in the RNC·SRP targeting complex (left panel) compared to the M-domain with bound signal sequence from the structures of the bacterial and archaeal M-domain complexed with the signal sequence (PDB:5NCO,4XCO, and 3KL4). The GM linker is colored slate blue. The location of the SRP GNRA tetraloop in the bacterial complex is shaded in black.

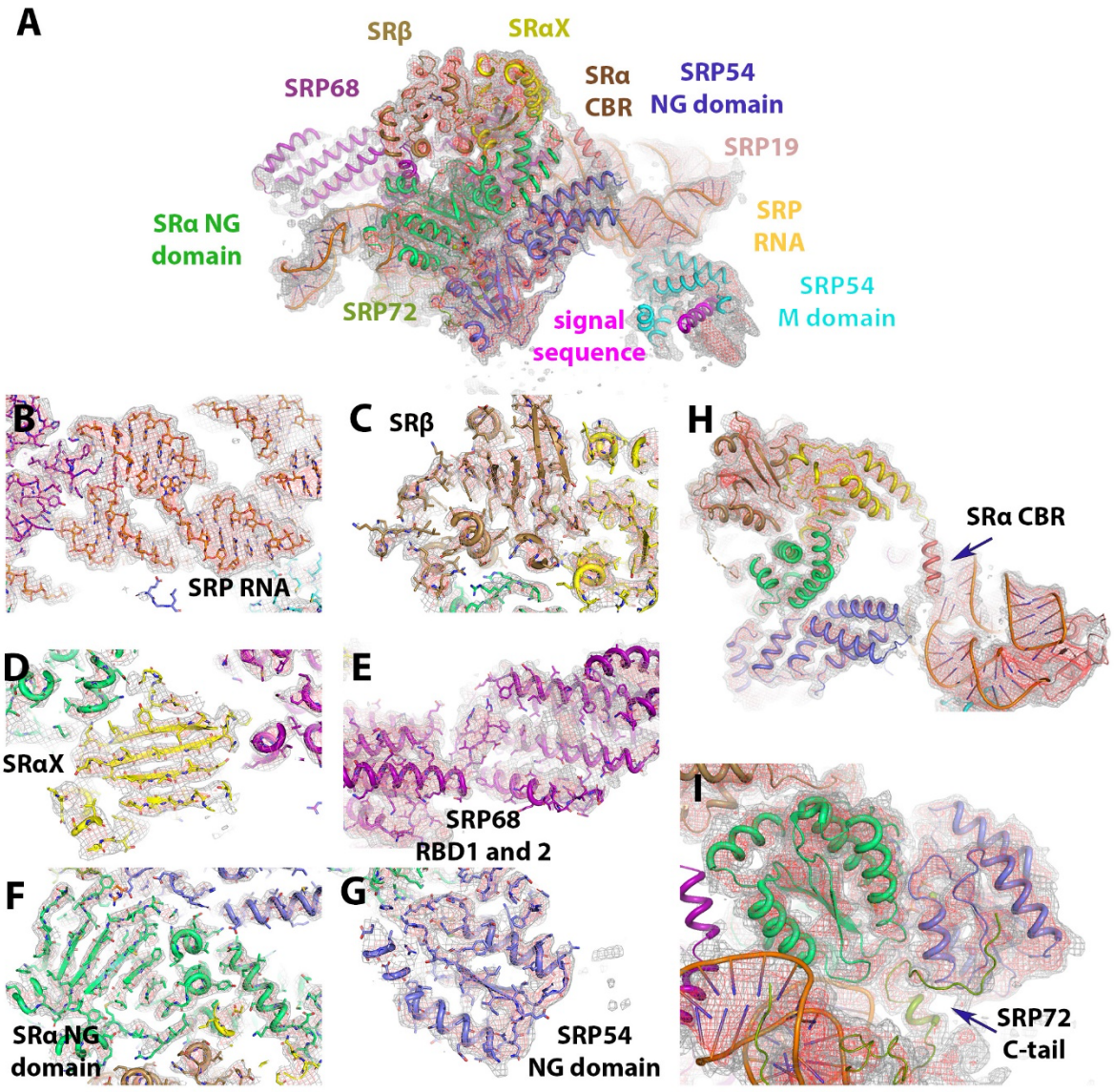

Figure S5. Representative cryo-EM densities of the mammalian SRP·SR targeting complex, Related to Figure 4.

(A) Overall EM-density of the SRP·SR at the SRP RNA distal site. **(B)** Close-up view of the SRP RNA density showing base separation with SRP68 (purple) in the vicinity. **(C)** Close-up view of the α helical insertion of SRP72 into the GTPases interface. **(D-G)** Representative EM-densities of SRα X, SRP68 RBD and SRP68 RBD2, SRα NG SRP54 NG, with fitted atomic model shown

as cartoon and sticks. **(H-I)** Representative views of the EM-densities sowing interactions between CBR and SRP72 tail with SRP RNA and SRP54, respectively. EM densities are shown as mesh at different contour levels and colored gray and red.

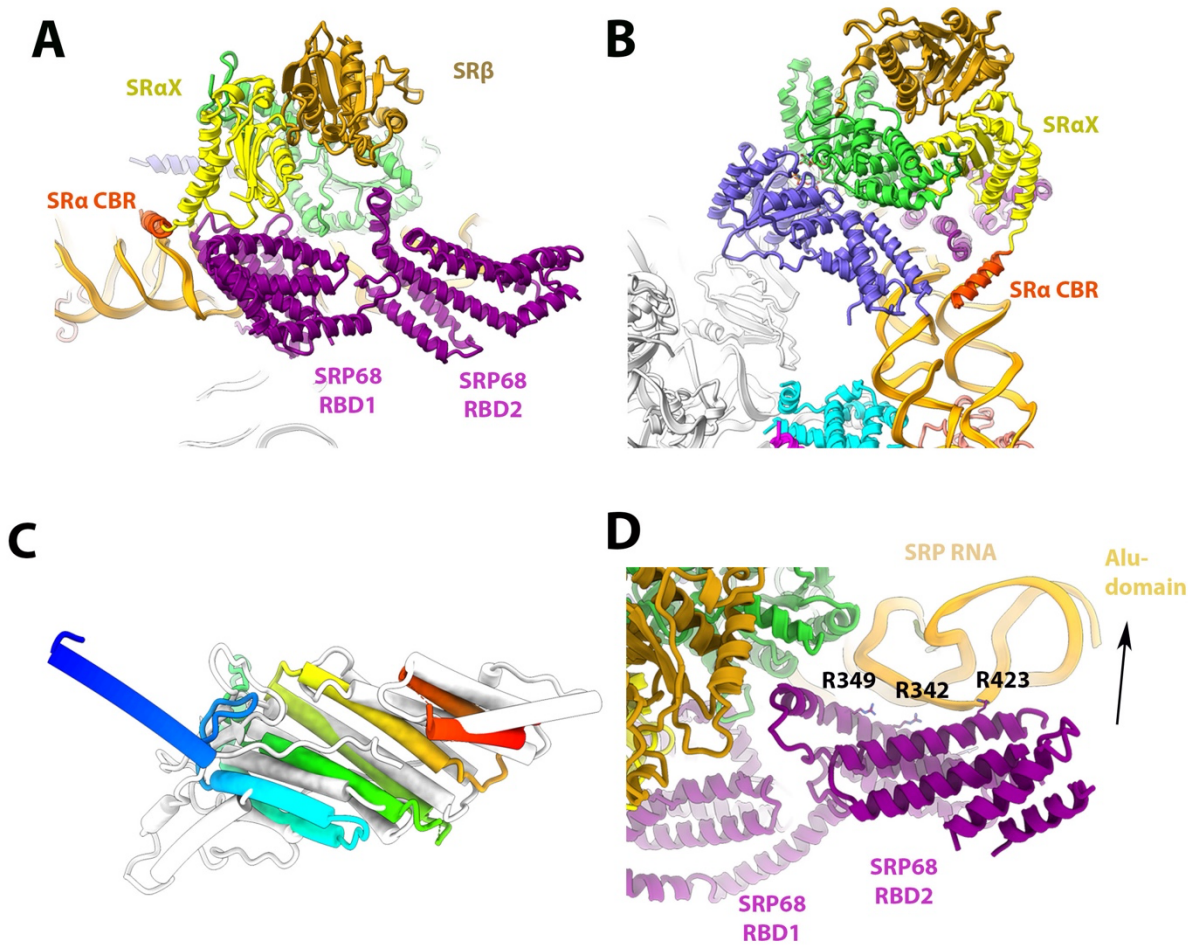

Figure S6. Overview of the SRP68 and SRα CBR interactions within SRP RNA, Related to Figure 4.

(A) Overview of the SRP68 structure depicting RBD1 and RBD2. **(B)** Overview of the SRα CBR interactions with the SRP RNA. **(C)** Overlay of SRP68 RBD2 and the x-ray structure of the Bro1 domain of Alix (PDB:2OEW) colored white. The SRP68 RBD is rainbow colored where the N and C termini are indicated. **(D)** Interaction of the SRP68 with the SRP RNA. Residues R352, R345, and R426 of SRP68 RBD2 are shown as sticks. SRP68 and SRP RNA and SR are shown as cartoon. Coloring scheme is the same as in Figure 1. Black arrow indicated the position of the Alu-domain of SRP RNA.

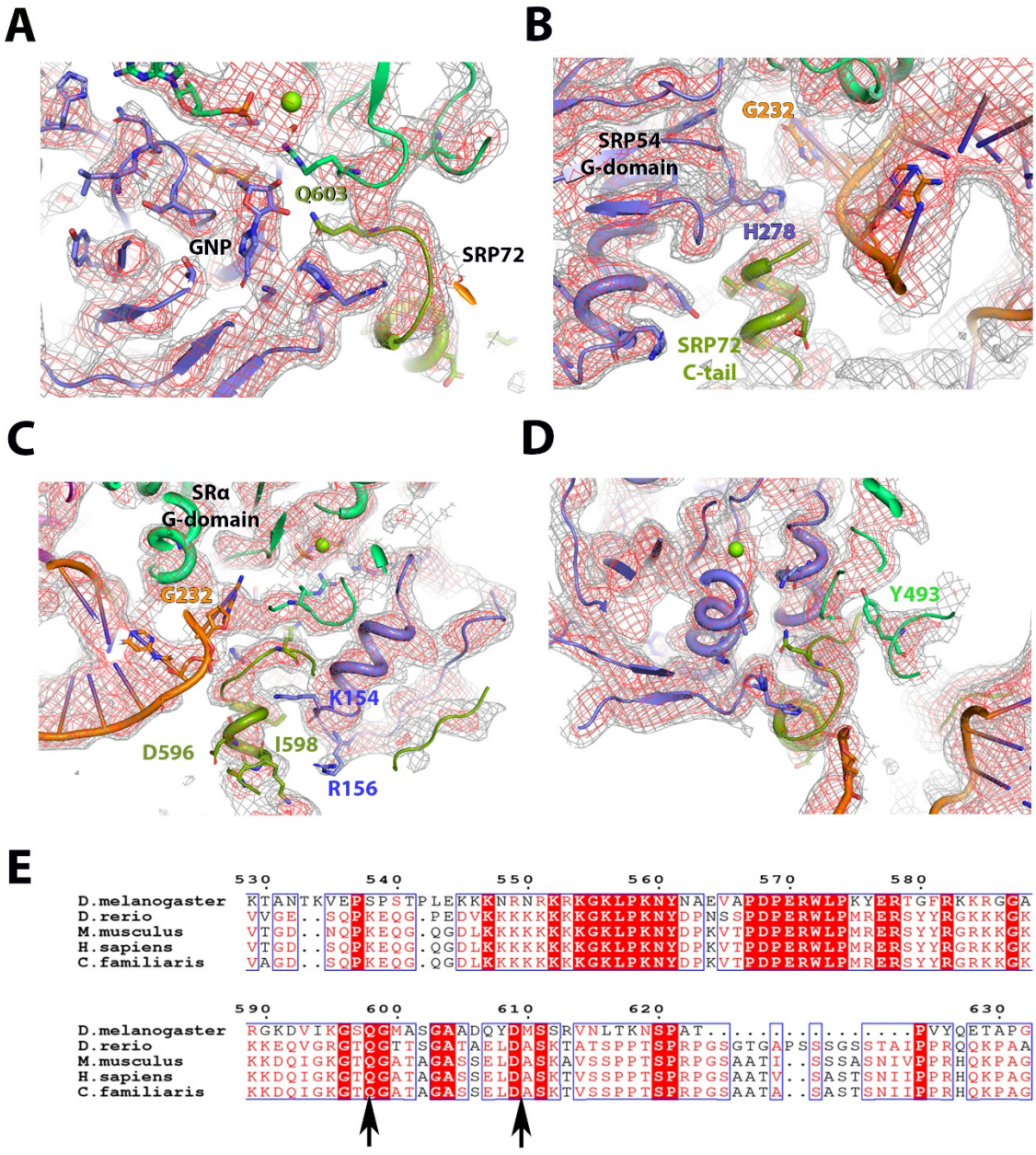

Figure S7. Molecular interactions of the SRP72 and the NG-heterodimer, Related to Figure 4 and 5.

(A-D) Representative views of the EM-densities of the SRP72 insertion and its interaction with the GDPPNP molecule and with SRP54 and SRα. Dashed line indicates the H-bonding distance

between the Q603 of SRP62 and the sugar moiety of the GDPPNP molecule bound to SRP54. Atomic models are shown as sticks and colored as shown in Figure 2. **(E)** Sequence alignment of the SRP72 protein across different organisms in eukaryotes. Arrows indicate the position of the conserved Q603 (human numbering), which is inserted into the SRP·SR GTPase interface and the caspase cleavage site that is observed interacting with the G-domain of SRP54.

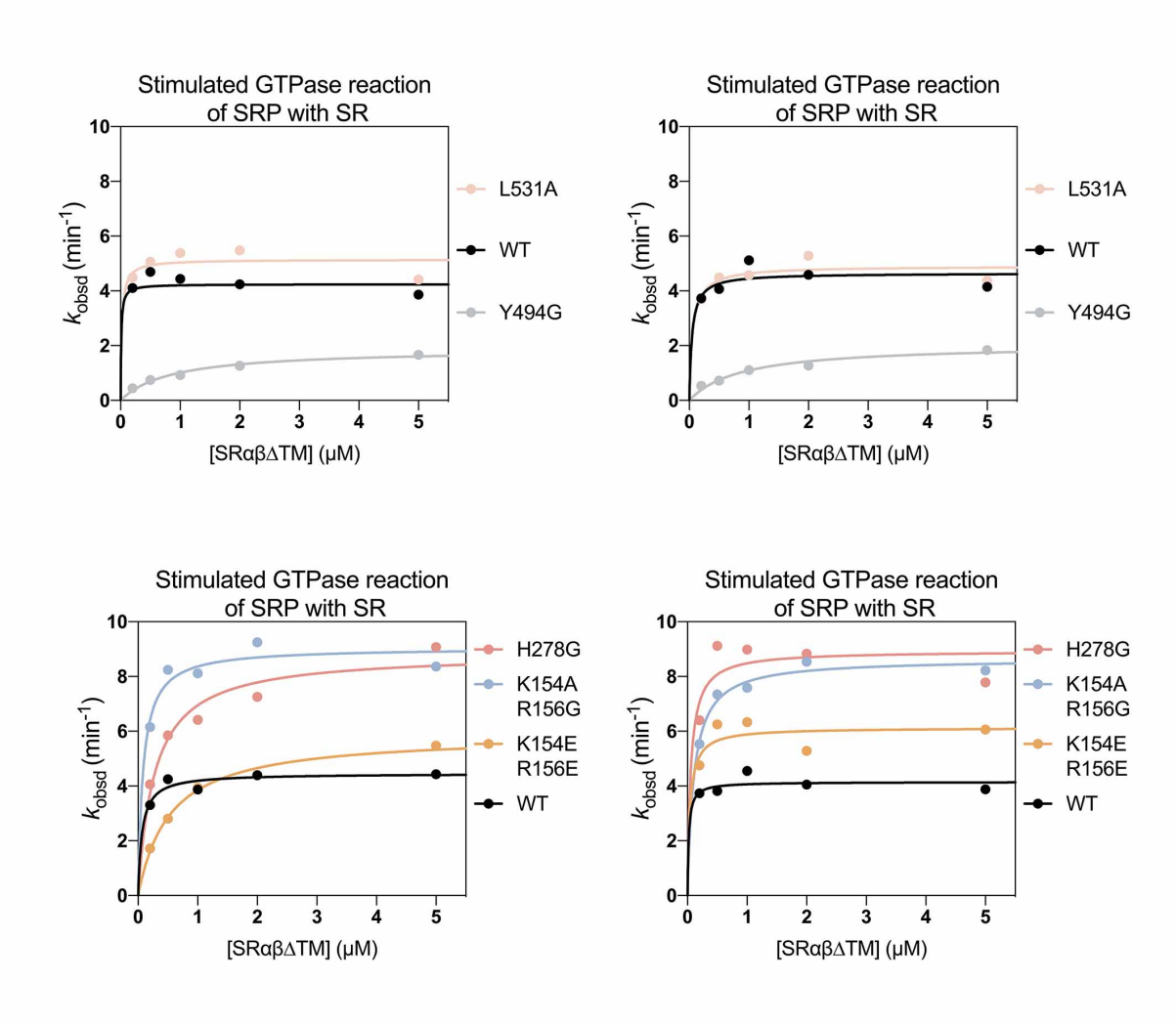

Figure S8 Representative Michaelis-Menten curves for the reciprocally stimulated GTPase reactions of SRP with SR, Related to Figure 4..

Observed GTPase rate constants (k_{obsd}) was measured as described in Materials and Methods. All reactions contained 200 nM wild type or mutant SRP fused to the signal sequence, indicated concentrations of wild type or mutant SRαβΔTM, 250 nM 80S ribosome, and 100 μM GTP doped with γ-^{32}P-GTP. The lines are fits of the data to the Michaelis-Menten equation, and the obtained values of k_{cat} are summarized in main Figure 4E. Data were reported as mean ± S.D., with n = 2-4.